

Multi-wavelength observations of an evolved galaxy group: An endpoint of galaxy merging?

L. R. Jones, T. J. Ponman and Duncan A. Forbes

School of Physics & Astronomy, University of Birmingham, Birmingham B15 2TT, UK.

11 August 2018

ABSTRACT

The group of galaxies RXJ1340.6+4018 has approximately the same bolometric X-ray luminosity as other bright galaxy groups and poor clusters such as the Virgo cluster. However, 70% of the optical luminosity of the group comes from a dominant giant elliptical galaxy, compared to 5% from M87 in Virgo. The second brightest galaxy in RXJ1340.6+4018 is a factor of 10 fainter ($\Delta m_{12}=2.5$ mag) than the dominant elliptical, and the galaxy luminosity function has a gap at about L^* .

We interpret the properties of the system as a result of galaxy merging within a galaxy group. We find that the central galaxy lies on the fundamental plane of ellipticals, has an undisturbed, non-cD morphology, and has no spectral features indicative of recent star formation, suggesting that the last major merger occurred $\gtrsim 4$ Gyr ago. The deviation of the system from the cluster $L_X - T$ relation in the opposite sense to most groups may be due to an early epoch of formation of the group or due to a strong cooling flow.

The unusual elongation of the X-ray isophotes and the similarity between the X-ray and optical ellipticities at large radii (~ 230 kpc) suggest that both the X-ray gas and the outermost stars of the dominant galaxy are responding to an elongated dark matter distribution. RXJ1340.6+4018 may be part of a filamentary structure related to infall in the outskirts of the cluster A1774.

Key words: galaxies: clusters: general - X-rays: galaxies - galaxies: elliptical

1 INTRODUCTION

If galaxy merging is a common process in the cores of galaxy groups, then there may be a population of ‘fossil’ groups in which most of the galaxies have merged, leaving a giant elliptical galaxy but few other galaxies. Galaxy groups represent one of the environments where galaxy mergers are predicted to happen most frequently, because of the relatively low velocity dispersion of the constituent galaxies compared to the velocity dispersion in clusters of galaxies. For example, in the numerical simulations of Barnes (1985, 1989) compact group members merge to form a single elliptical galaxy within a few billion years. In hierarchical models of structure formation, isolated galaxy groups are predicted to be relatively old systems, so that there has been a long period over which merging could occur.

The first candidate fossil galaxy group, RXJ1340.6+4018, was discovered via its extended X-ray emission by Ponman et al (1994; hereafter P94). The X-ray properties of the system, including its bolometric X-ray luminosity (4.5×10^{43} erg s⁻¹), temperature (0.92 ± 0.08 keV) and extent (core radius 140-

390 kpc), are similar to those of well known X-ray bright galaxy groups (e.g. Mulchaey et al 1996). The X-ray luminosity and extent are at least an order of magnitude higher than those of normal elliptical galaxies. However, P94 detected no excess of galaxies in projection on the sky near the X-ray position; only a single luminous ($M_V = -23.5$ mag) elliptical galaxy was coincident with the X-ray peak. The explanation suggested by P94 was that the former group galaxies had merged, creating the single luminous elliptical galaxy and leaving a halo of X-ray emitting gas and dark matter.

In a recent study, Vikhlinin et al (1999) find three very similar systems, in addition to independently discovering RXJ1340.6+4018, and find that the space density of such groups is similar to that of luminous field ellipticals with $L > 6L^*$ ($M_R < -22.5$). Thus a large fraction of luminous field ellipticals may be the result of galaxy merging in groups. X-ray observations of an optically-selected isolated elliptical galaxy by Mulchaey & Zabludoff (1999) also revealed a system with the X-ray properties of a group, lending support to this idea.

In this paper we investigate the properties of

RXJ1340.6+4018 in more detail and assess the evidence for it being a result of galaxy merging. If it is an old merger remnant then comparison with typical ellipticals gives a valuable check on the idea that many ellipticals are the result of mergers. The detection of an overluminous X-ray halo containing only one bright (elliptical) galaxy may be one of the few ways of identifying such evolved systems.

In Section 2 we describe new optical imaging and spectroscopy and high resolution X-ray observations of the RXJ1340.6+4018 field. The results of isophotal, photometric and dynamical analyses of the central galaxy and its environment are described in Section 3. A comparison with other galaxy systems and a discussion of the possible history of this system are given in Section 4. The last Section contains the concluding remarks. We assume $H_0=50h_{50}$ $\text{km s}^{-1} \text{Mpc}^{-1}$ and $q_0=0.5$ throughout (as done by P94).

2 OBSERVATIONS

2.1 Optical Observations

2.1.1 Redshifts of nearby galaxies

Low resolution spectra of RXJ1340.6+4018 and objects close to it on the sky were obtained at the Kitt Peak 2.1m telescope on January 21st 1996. A finding chart is shown in Fig. 1. Two slit positions were used. At one, spectra of objects G2, G9, G7 & S4 were obtained (position angle 79° ; exposure 60 min). The star S4 is outside the area of Fig. 1, to the east. At the other slit position spectra of objects G1, G3 and G5 were obtained (position angle 71° ; exposure 30 min). Object G1 is the central, luminous elliptical galaxy. The second slit was aligned on galaxies G3 & G5 and so did not quite cross the core of G1, but passed 2 arcsec south of the core. The Goldcam spectrograph and Ford 3kx1k CCD were used with a slitwidth of 2.5 arcsec and a grating of 300 lines/mm, giving a resolution of 10\AA (FWHM). Arc lamp, flat field and F8 star exposures (the latter for the removal of atmospheric absorption features) were obtained with the telescope at or near the position of RXJ1340.6+4018. Spectra of flux standard stars were obtained during the night. Standard IRAF reduction procedures were used and redshifts were determined from Gaussian fits to 4-8 absorption lines per galaxy. Redshift errors were determined from the dispersion in the individual line measurements. The redshifts are listed in Table 1.

The redshift of G1 ($z=0.1716$) agrees with the measurement of P94. Three of the other galaxies observed (G2, G3 and G5) have redshifts very close to that of G1 ($\Delta v < 450 \text{ km s}^{-1}$). The spectra of all four of these galaxies are typical of elliptical galaxies. Two objects (G7 & G9) are background galaxies and one object (S4) is a Galactic star. The only emission lines detected were unresolved [OII]3727 in the background galaxies G7 and G9, a common feature in faint field galaxies.

2.1.2 Internal velocity dispersion of the luminous galaxy

A higher resolution, high signal-to-noise spectrum of the brightest galaxy G1 was obtained at the Keck II telescope on May 2nd 1998. The observation was made through thick cloud and so no flux standards were observed. The low

Table 1. Redshifts of galaxies in the RXJ1340.6+4018 field

Galaxy	α (J2000)	δ	z	R [†]
G1	13 40 32.80	40 17 39.7	0.1716 ± 0.0003	16.1
G2	13 40 32.49	40 18 9.9	0.1705 ± 0.0002	18.6
G3	13 40 31.27	40 17 31.2	0.1700 ± 0.0006	18.9
G5	13 40 26.64	40 17 13.1	0.1734 ± 0.0006	19.2
G7	13 40 39.25	40 18 25.4	0.3033 ± 0.0002	18.7
G9	13 40 37.43	40 18 22.2	0.3087 ± 0.0004	19.2

[†] total magnitude

resolution imaging spectrograph (LRIS), a grating of 600 lines/mm and a slitwidth of 1.5 arcsec were used to give a resolution of 6.7\AA (FWHM), corresponding to $\sigma \approx 140 \text{ km s}^{-1}$. The slit was aligned across the galaxy core at a position angle of 90° . Arc lamp and flat field exposures were obtained immediately after the target exposure. Standard IRAF reduction procedures resulted in the spectrum shown in Fig. 2 which was extracted from a 2.2 arcsec section along the slit, centred on the galaxy core. The signal-to-noise in the reduced spectrum is ≈ 30 per 1.2\AA pixel.

The redshift of $z=0.1724 \pm 0.0002$, derived from Gaussian fits to 9 absorption lines, is consistent (within 2σ) with that derived from the Kitt Peak 2.1m spectrum. The velocity dispersion in the galaxy core was measured from Gaussian fits to the four absorption lines which had equivalent widths $> 1\text{\AA}$ but were not blended with nearby strong lines (a Fourier analysis was not possible because no template stars were observed with the same grating). These four lines were Fe 4383, Ca 4455, Fe 5270 and H β . The observed weighted mean line width was $\sigma=320 \pm 40 \text{ km s}^{-1}$. The strong NaD lines could not be used because they were contaminated by the O₂ B-band atmospheric absorption feature. Although the Mg β triplet was not resolved, a fit with three fixed line centres and a single variable line width and a variable continuum gave a line width ($\sigma=350 \pm 30 \text{ km s}^{-1}$) consistent with the results from the other four lines. Errors on the line widths were estimated via 100 Monte-Carlo simulations for each line. After correcting for the instrumental broadening, the weighted mean line width was $\sigma_0=260 \pm 30 \text{ km s}^{-1}$.

2.1.3 Deep optical imaging

Images of RXJ1340.6+4018 in the R and B bands were obtained in service time at the Isaac Newton 2.5m Telescope (INT) on January 25-26th 1995. A Tektronix 1024x1024 CCD was used at prime focus, resulting in a pixel size of 0.59 arcsec and field of view of 9.8×9.8 arcmin. The seeing was 1.2 arcsec FWHM. Exposures of 6x600s in R and 3x500s in B were obtained over the two nights, moving the telescope slightly between exposures to facilitate flat-fielding. A flat-field image was initially made from a combination of 6 twilight sky images. Application of this flat-field image to the target images left a residual gradient in the sky of $< 0.2\%$ over the full 9.8 arcmin frame width. The three frames with the worst residual gradient (which were those for which no twilight flats were obtained on the same night as the target data) were additionally flat-fielded by a smoothed ‘sky flat’ created by a median combination of the three origi-

Figure 1. R band CCD image of the central region of the group RXJ1340.6+4018, showing the giant elliptical galaxy G1 and other galaxies in the field. Galaxies G2, G3 & G5 are in the galaxy group dominated by galaxy G1; G7 & G9 are background galaxies. The faint galaxy G10, 9'' W of the centre of G1, is unusually blue (its redshift is unknown). A bright star is marked with an "S". North is up and east is left. The image is 2.5 arcmin across (570 h_0 kpc at the redshift of RXJ1340.6+4018). The intensity scaling is log(square root).

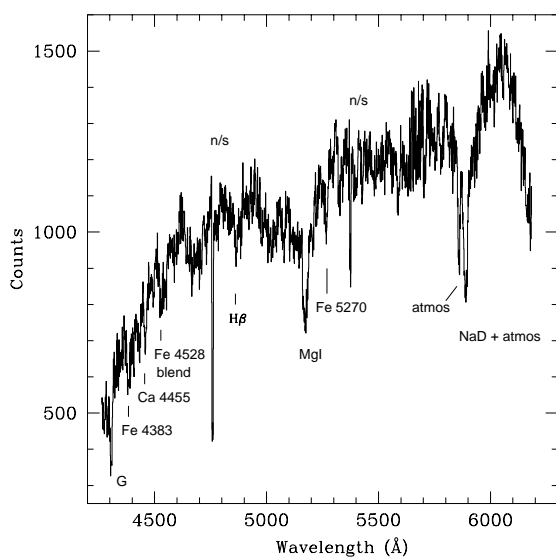


Figure 2. Spectrum of the dominant galaxy G1 shifted to rest wavelengths. Prominent absorption lines and incompletely subtracted night sky lines are marked.

Figure 3. R band CCD image and overlaid X-ray contours from the ROSAT PSPC and ROAST HRI (dashed). The X-ray contours are at logarithmic intervals of a factor of 1.4 in surface brightness.

nal frames. This operation was designed to remove the large scale gradient. The sky in the resulting images was flat to within $<0.1\%$ across the full extent of each frame (corresponding to $R>28$ mag arcsec $^{-2}$). The final R band image from the six frames combined is shown in Fig. 3.

The INT images were obtained in slightly non-photometric conditions, so photometric calibration was performed via the Nordic Optical 2.5m Telescope (NOT) images of the same field described in P94 in the R band, but was unavailable for the B band. Here we give a brief description of the V and R photometry employed at the NOT. The photometry was on the Johnson (V) and Kron-Cousins (R) system. The NOT images were not as deep as those described here, but were obtained under photometric conditions, as measured by 12 observations of Landolt (1992) and Christian et al (1985) standard star fields in V and R throughout the night. These standard star measurements were consistent with standard atmospheric extinction corrections of $0.06\sec(z)$ in R and $0.10\sec(z)$ in V, where z is the airmass. Colour terms of $0.0(V-R)$ in R and $0.34(V-R)$ in V were derived from 17 stars (in R) and 4 stars (in V). Several standard stars were of very similar V-R colour to galaxy G1. We estimate the NOT photometry to be accurate to 0.05 mag. Calibration of the deep INT image was achieved via a simple comparison with the NOT R photometry for the brightest 8 galaxies (including those with measured redshifts) within a 6.6 arcsec radius aperture, and was accurate to 0.03 mag (1 σ random error).

Figure 4. Azimuthally averaged X-ray surface brightness profiles. X-ray emission is detected to a radius of $\gtrsim 0.1^\circ$ or $1.3 h_{50}^{-1}$ Mpc. *ROSAT* PSPC data are shown as crosses and scaled HRI data as points. The PSPC/HRI count rate ratio used to scale the HRI data was predicted using the spectral parameters measured from the PSPC spectrum.

lution of 5 arcsec (FWHM), and is reasonably sensitive to point-like X-ray sources, but because of a higher unrejected particle background and lower quantum efficiency, it is not as sensitive to faint diffuse X-ray emission as the *ROSAT* position sensitive proportional counter (PSPC) which was used by P94. Nevertheless, an extended source was detected in the HRI at the position of the peak of the PSPC emission (see the dashed contours in Fig. 3). The position of the HRI image was updated by 5 arcsec by comparing the X-ray positions of 5 point sources in the HRI image with the positions of optical counterparts from Palomar plate measurements. The PSPC data is subject to a systematic positional uncertainty of ≈ 10 arcsec. No point X-ray sources were detected in the HRI image within the PSPC contours of Fig. 3, showing that the extended emission detected with the PSPC by P94 (with a poorer spatial response $FWHM \approx 25$ arcsec) is from a truly diffuse source, and not from a superposition of unresolved point sources. Any non-variable point source with a flux of 10% of the total flux of RXJ1340.6+4018 would have been detected with a significance of at least 5σ in the HRI observation.

The combined HRI and PSPC azimuthally averaged surface brightness profiles are shown in Fig. 4. X-ray emission is detected to a radius of $\gtrsim 0.1^\circ$ or $1.3 h_{50}^{-1}$ Mpc. In the figure, the HRI surface brightness has been scaled up by a factor of 3.78, corresponding to the predicted PSPC/HRI count rate ratio for a thermal plasma spectrum as determined by P94 ($T=0.92$ keV, metallicity=0.36 solar, $N_H=7.4 \times 10^{19}$ cm $^{-2}$). The PSPC surface brightness profile is consistent with the HRI profile in the overlap region, and consistent with a smooth extrapolation of the HRI profile, again suggesting that unresolved point sources do not make a significant contribution to the PSPC flux.

Figure 5. The same field as shown in Fig. 3, after subtraction of an elliptical model fit to galaxy G1 as described in the text. There are few, if any, residual features.

2.2 X-ray Observations

RXJ1340.6+4018 was observed with the *ROSAT* High Resolution Imager (HRI) for a total of 51 ksec in December 1994 and June 1995. The HRI count rate was 2.9×10^{-3} ct s $^{-1}$ within a radius of 1.2 arcmin. The HRI has a spatial reso-

3 ANALYSIS AND RESULTS

3.1 The nature of the system

The luminous elliptical galaxy coincident with the peak of the X-ray emission is not completely isolated, but has at least three faint companion galaxies with measured redshifts. The system is a group of galaxies, and the diffuse X-ray emission originates in an intra-group medium (IGM). The group, however, has an unusually optically luminous central galaxy and an unusually large magnitude gap between the brightest and second brightest galaxies. Here we determine the properties of both the central galaxy and the galaxy group. The group properties are summarized in Table 2.

3.2 Group luminosity function

The luminosity function of the galaxies in the group was estimated using a simple statistical method. The surface density of field galaxies surrounding the group was subtracted from the surface density of galaxies located in a circular region centred on the group, as a function of magnitude. Photometry of both field and group galaxies was based on analysis of the deep R band INT CCD image using the Starlink PISA package (Draper & Eaton 1996). The image used for source detection was that with the bright elliptical galaxy subtracted (Fig. 5; see Section 3.4), so as to avoid spurious faint sources being produced in the noisy, low surface brightness outer parts of the galaxy profile, and to include sources projected on to the bright galaxy. Regions around four bright stars were also excluded from the analysis, again to avoid spurious source detections. An isophotal threshold of $26.6 \text{ R mag arcsec}^{-2}$ (2σ per pixel above sky) was used, with a minimum of 4 connected pixels above the threshold, to define source detections. A total of 2577 objects were found in an area of 55.1 arcmin^2 . The bright central galaxy was inserted manually into the object list.

Photometry was performed using an asymptotic curve of growth analysis for each object as described by Kron (1980). Star-galaxy separation was performed, following Jones et al (1991), using a $\log(\text{area})$ -magnitude plot for $R < 18$ and a $\log(I_{\text{peak}})$ -magnitude plot for $18 < R < 26$, where the area is the isophotal area above the threshold, and I_{peak} is the peak surface brightness. The completeness level was estimated from galaxy counts in a background region, defined as the area of the image $> 1.8 \text{ arcmin}$ ($400 \text{ h}_{50}^{-1} \text{ kpc}$) from the centre of the galaxy G1. The background galaxy counts start to turn over at $R=24$ mag, and we take this as the completeness limit (see Fig. 6). The background galaxy counts are consistent with field galaxy counts of Jones et al (1991) to their limit of $R=22$, and slightly higher than the measurements of other authors at $22 < R < 24$ (but within 2.1 times the one-sigma fluctuation amplitude measured by Metcalfe et al 1991 in a similar size field). This small excess may be due to the effects of the large-scale structure in the region (perhaps associated with Abell 1774).

Our background galaxy counts predict 207 field galaxies within a 1.8 arcmin radius circle at $R < 24$; we measure 250 galaxies within the same radius circle centred on galaxy G1, giving an excess of 43 ± 16 galaxies within a radius of $400 \text{ h}_{50}^{-1} \text{ kpc}$. Within $200 \text{ h}_{50}^{-1} \text{ kpc}$ radius the excess is

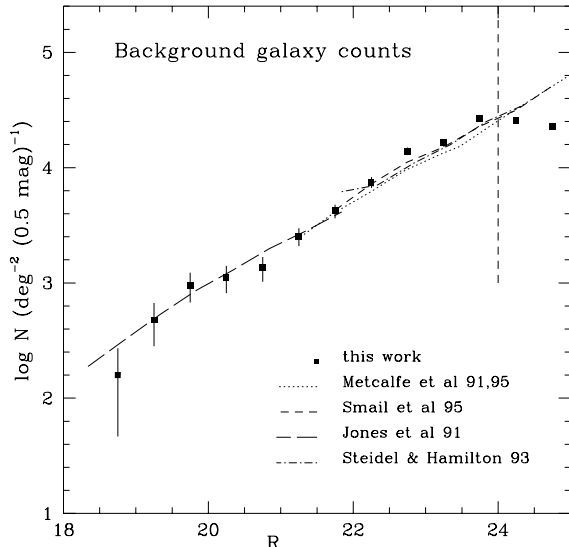


Figure 6. Background galaxy counts at radii $> 400 \text{ h}_{50}^{-1} \text{ kpc}$ from the centre of the RXJ1340.6+4018 group. The limit of completeness is shown by the vertical line. Field galaxy counts of other authors are shown as dashed lines. The counts of Steidel & Hamilton (1993) have been transformed to the R band using $R = R - 0.14$.

26 ± 8.8 galaxies. Using the field galaxy counts of Metcalfe et al (1991, 1995) would increase the number of group galaxies within $400 \text{ h}_{50}^{-1} \text{ kpc}$ to 71 ± 16 , an increase of a factor of 1.7, and an indicator of the likely level of systematic error in the luminosity function.

K-corrections for an elliptical galaxy at $z=0.171$ of $K_B=0.84$, $K_V=0.32$ (Pence 1976) and $K_R=0.17$ (Metcalfe et al (1991); Saglia et al (1997)) were assumed. A Galactic extinction of $A_B < 0.06$ mag was obtained from Burstein & Heiles (1984). Converting the neutral hydrogen column density of $N_H=7.4 \times 10^{19} \text{ cm}^{-2}$ to an extinction using the relation of Jenkins & Savage (1974) gives $A_B=0.04$ mag (or $A_R=0.02$ mag). As these values are less than our photometric errors, we have assumed that the Galactic extinction is zero.

The group luminosity function is shown in Fig. 7. The luminosity function was constructed using the background counts derived from the same image as the group counts, in order to have consistent depth, galaxy detection parameters and photometry. A bin size of one magnitude has been used in Fig. 7. The large magnitude gap Δm_{12} between the brightest galaxy and the second brightest galaxy is clear in this figure (the value is $\Delta m_{12} = 2.5$ mag). The unusually high luminosity of the brightest galaxy when compared to the LFs of other clusters and groups is also evident.

The LFs of other systems shown in Fig. 7 are representative of the LF shape in groups and poor clusters. Their detailed normalization should not be compared because they have been measured from different projected areas in each system. In addition, the Virgo LF has been rescaled by a factor of 0.1 in order to compare its shape with the LF of RXJ1340.6+4018.

Table 2. Properties of the RXJ1340.6+4018 group

Redshift	$z=0.1710 \pm 0.0007$
Velocity dispersion	$\sigma_r=380 (+350, -110) \text{ km s}^{-1}$
Bolometric X-ray luminosity [†]	$4.5 \times 10^{43} h_{50}^{-2} \text{ erg s}^{-1}$
X-ray temperature [†]	$T=0.92 \pm 0.08 \text{ keV}$
IGM X-ray metallicity [†]	$Z=0.36 (+0.15, -0.11) \text{ solar}$
Magnitude gap (in R)	$\Delta m_{12}=2.5 \text{ mag}$
Central galaxy surface density	$N_{0.5}^c=2.8$
Total gravitating mass ($r < 340 \text{ kpc}$) [†]	$2.8 \times 10^{13} h_{50}^{-1} M_\odot$
Virial mass [‡]	$6.1 \times 10^{13} h_{50}^{-1} M_\odot$

[†] from Ponman et al (1994)

[‡] The virial mass is poorly constrained because of the small number of measured galaxy velocities.

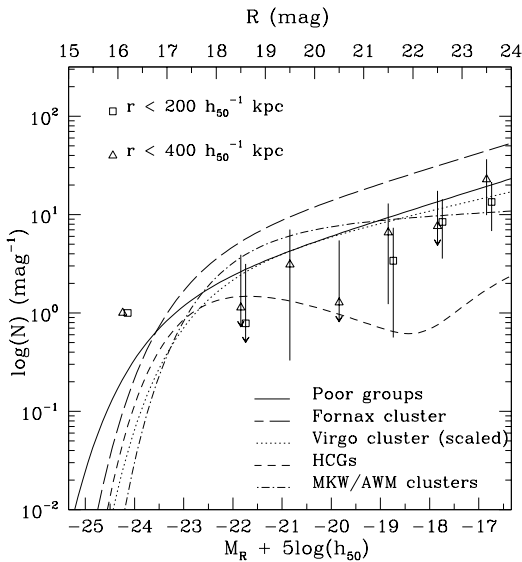


Figure 7. Galaxy luminosity function of the RXJ1340.6+4018 group, for galaxies within two different radii (shown as triangular and square symbols). The large magnitude gap between the brightest galaxy (G1; $M_R=-24.2$) and the second brightest ($M_R=-21.7$) is evident, as is the low likelihood of other clusters & groups containing a galaxy as luminous as this. The other luminosity functions (shown as continuous lines) are taken from Ferguson & Sandage (1991) except for the Hickson compact group (HCGs) LF which is taken from Hunsberger, Charlton & Zaritsky (1998) (scaled to $H_0=50$) and the MKW/AWM poor cluster LF which is taken from Yamagata & Maehara (1986). Colour transformations to the R band assumed B-R=1.5 mag for the Ferguson & Sandage results and V-R=0.6 for Yamagata & Maehara. Only the Virgo cluster LF has been scaled in number (by a factor of 0.1).

3.3 Group velocity dispersion and dynamical mass

The redshift and line-of-sight velocity dispersion (σ_r) of the group of galaxies was estimated from the four available galaxy redshifts. For small sample sizes, Beers et al. (1990) found that the median redshift and simple Gaussian dispersion give the best estimates. Adopting this method gives a group redshift of $z=0.1710 \pm 0.0007$ and a velocity dispersion $\sigma_r=380 (+350, -110) \text{ km s}^{-1}$ where the velocity dispersion has been corrected for cosmological effects and redshift measurement errors, and its error has been calculated as

described by Danese et al. (1980). Zabludoff & Mulchaey (1998) note that group velocity dispersions measured from a small number of centrally concentrated brightest galaxies usually underestimate the true velocity dispersion, as measured from a much larger sample, by a factor ~ 1.5 . The kinematic quantities derived from the velocity dispersion are of dubious value, because they were based on only 4 galaxy velocities and positions, and those 4 galaxies were concentrated towards the centre of the group. With this caveat, we calculate a virial mass using the standard equations as given by Ramella et al (1989). For a virial radius of 310 kpc and a mean projected galaxy separation of 330 kpc, we find a virial mass of $6.1 \times 10^{13} M_\odot$.

3.4 Isophotal analysis and photometry of the central galaxy

In order to determine if the central elliptical galaxy G1 shows any deviations from an elliptical shape and to measure its photometric properties, we used the ISOPHOTE package in IRAF to fit elliptical isophotes to the deep R band image, using the algorithm of Jedrzejewski (1987). The regions around several stars and galaxies close to G1 on the sky were ignored in the fitting. The galaxy profile could be followed to a maximum semi-major axis length (a) of 62 arcsec or $230 h_{50}^{-1} \text{ kpc}$. The surface brightness values were corrected for K-corrections and $(1+z)^4$ surface brightness dimming. The R band image after subtraction of the best-fit elliptical model is shown in Fig. 5. This image reaches a limiting surface brightness of $\mu_R > 26 \text{ mag arcsec}^{-2}$, considerably fainter than, for example, the tidal tails in NGC 7252, a 1 Gyr old merger remnant ($\mu_R \approx 25 \text{ mag arcsec}^{-2}$; Hibbard et al 1994). However, no diffuse residual features are visible in this image; only a few galaxies and a stellar object near the galaxy centre are visible. While the two features closest to the galaxy centre may be multiple nuclei, they may also be a faint galaxy and a star observed in projection against the central galaxy. The high number density of similarly faint objects throughout the image suggests that they may be unrelated to the central galaxy. The small feature at the galaxy core is an artifact of the imperfect fit in the central region due to seeing effects.

The surface brightness as a function of $a^{1/4}$ is shown in Fig. 8. The straight line, indicative of a de Vaucouleurs $r^{1/4}$ profile with an effective semi-major axis of $a_e=10.6 \pm 0.6 \text{ arcsec}$, is a good fit in the range $3.0 < a < 54 \text{ arcsec}$, ie. outside the central region affected by the seeing ($\chi^2=18.0$ for 23

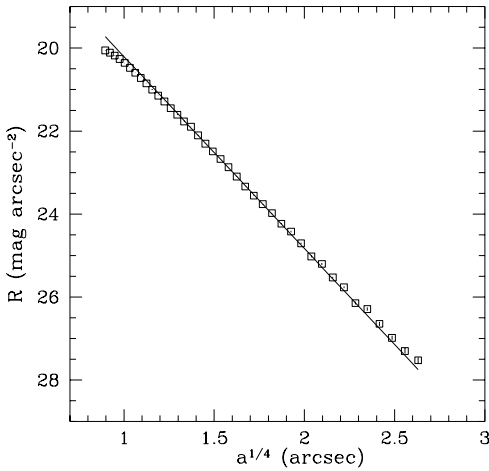


Figure 8. R band surface brightness of the dominant galaxy G1 as a function of $(\text{semi-major axis})^{1/4}$, from a fit to elliptical isophotes. A pure de Vaucouleurs $r^{1/4}$ profile (solid line) is a good description outside the central region affected by the seeing.

degrees of freedom). An effective radius, r_e , of 6.4 ± 0.3 arcsec, is obtained from a de Vaucouleurs profile fit to $r=\sqrt{ab}$ over the range $3.0 < r < 36$ arcsec. This value of r_e is consistent with that found by P94. The B band image is of lower signal-to-noise than the R band image, but following the same procedure again gave a profile consistent with a $r^{1/4}$ law, with $a_e=13.8 \pm 3.0$ arcsec and $r_e=7.8 \pm 0.9$ arcsec.

The variation of ellipticity with semi-major axis is given in Fig. 9. Here ellipticity is defined as $e=1-b/a$. The ellipticity increases monotonically with radius from $e=0.1$ (ie. near circular) to $e=0.5$ (axis ratio b/a of 0.5). This range of ellipticity within individual luminous elliptical galaxies is not unusual, although galaxies with similarly large ranges of ellipticity also usually have disk or dust lane features which affect the isophotal analysis (eg. Goudfrooij et al 1994). The position angle of the major axis is approximately constant between 20° and 25° . The amplitude of the 4th cosine harmonic measures ‘boxy’ or ‘disky’ deviations from perfect ellipticity in the isophotes. The value of this amplitude is consistent with zero at all radii outside the central seeing-affected region, implying that no significant deviations are present, at least in our data.

Total magnitudes of the galaxy were measured by summing the light within a radius of $5.6r_e$ and adding a correction of 0.1 mag given by the $r^{1/4}$ profile for the light outside this radius. The total magnitudes are given in Table 3.

No photometric calibration was available for the B band. An approximate calibration was performed by assuming that the rest $(B-V)_0$ colour of galaxy G1 (at $r < 16$ arcsec) was $(B-V)_0=0.95$, given by the colour-central velocity dispersion relation for elliptical galaxies of Forbes, Ponman & Brown (1998).

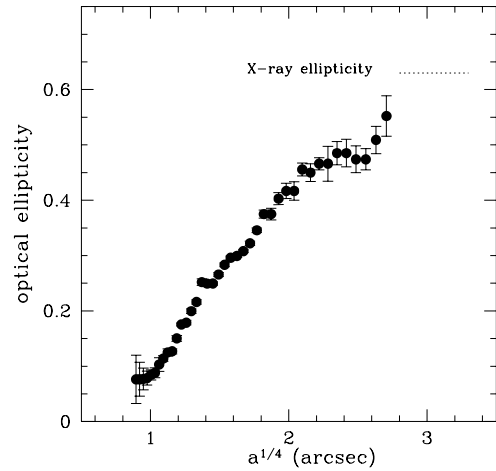


Figure 9. Ellipticity of the dominant galaxy G1 as a function of $(\text{semi-major axis})^{1/4}$, from a fit to elliptical isophotes. The ellipticity increases from near-circular at small radii to approach the X-ray ellipticity, shown by a dotted line, at large radii.

3.5 Fundamental Plane and Scaling Relations

If the luminous central galaxy is a result of recent multiple mergers, then its photometric and dynamical properties may not have yet relaxed to those of typical ellipticals. For normal ellipticals, these properties are defined by the fundamental plane.

In order to test if the central galaxy G1 lies on the fundamental plane of elliptical galaxies, the central velocity dispersion, the effective radius and the mean surface brightness are required. To compare with the fundamental plane of Djorgovski & Davis (1987), we used their definitions: the effective semi-major axis a_e from $r^{1/4}$ profile fits and the mean surface brightness $\langle \mu \rangle$ within a_e in the Lick r_G band. We used $H_0=100 \text{ km s}^{-1} \text{ Mpc}^{-1}$ to be consistent with Djorgovski & Davis (1987) (as opposed to the value of $H_0=50 \text{ km s}^{-1} \text{ Mpc}^{-1}$ used throughout the rest of this paper). The R band measurements (on the Kron-Cousins system) were converted to the Lick r_G band via the equations given in Djorgovski (1985) and Bessel (1979). The values found ($a_e=20 \pm 1.1 \text{ h}_{100}^{-1} \text{ kpc}$, $\langle \mu \rangle_{r_G}=21.37 \text{ mag arcsec}^{-2}$ and $\sigma_0=260 \pm 30 \text{ km s}^{-1}$) lie almost exactly on the fundamental plane relation of Djorgovski & Davis (1987) and are certainly consistent with the galaxy G1 being on the fundamental plane within our measurement errors.

We tested for consistency using the B band fundamental plane parameters, as given in Table 3. The galaxy was again found to lie on the fundamental plane, defined in the B band by the data of Prugniel & Simien (1996).

The Mg₂ absorption line index is an age/metallicity indicator. The index, as defined by Dressler (1984) and Faber et al. (1977), is the depression, in magnitudes, of the intensity at wavelengths 5157-5198Å compared to continuum sidebands. The mean value from the KPNO 2.1m spectrum and the Keck spectrum was 0.30 ± 0.15 . This value is consis-

Table 3. Properties of the central elliptical galaxy G1

total magnitude	R=16.1 $M_R=-24.2 + 5\log(h_{50})$ $M_V=-23.4 + 5\log(h_{50})$
type	E5
rest-frame colour ($r < 50$ kpc)	$(V-R)_0=0.72 \pm 0.06$
central velocity dispersion	$\sigma_0=260 \pm 30$ km s $^{-1}$
effective radius (R)	$r_e=6.4 \pm 0.3$ arcsec = 24.1 ± 1.1 h_{50}^{-1} kpc
effective radius (B)	$r_e=7.8 \pm 0.9$ arcsec = 29.4 ± 3.4 h_{50}^{-1} kpc
effective semi-major axis (R)	$a_e=10.6 \pm 0.6$ arcsec = 40.0 ± 2.3 h_{50}^{-1} kpc
effective semi-major axis (B)	$a_e=13.8 \pm 3.0$ arcsec = 52.0 ± 11.3 h_{50}^{-1} kpc
Mean surface brightness	$\mu_R=21.68$ mag arcsec $^{-2}$
within a_e (corrected)	$\mu_{r_G}=21.37$ $\mu_B=23.65$ mag arcsec $^{-2}$ \dagger
Mg ₂ index ‡	0.30 \pm 0.15
Radio power at 1.5 GHz ‡	3.5×10^{30} erg s $^{-1}$ Hz $^{-1}$

 \dagger from Ponman et al (1994) \ddagger accurate to ≈ 0.3 mag in B. § Mg₂ index as defined in Dressler (1984) and Faber et al (1977).

tent with the elliptical Mg₂- σ_0 relation of Bender, Burstein & Faber (1993), where σ_0 is the central velocity dispersion. We also note that the measured rest-frame (V-R)₀ colour of the galaxy is consistent with the colour-magnitude relation of Prugniel & Simien (1996).

3.6 Neighbouring galaxy properties

If galaxy merging is an important process, then there may be signs of it in galaxies close to the group centre. The colours and mean surface brightnesses of galaxies at a range of projected radii from the dominant galaxy were measured and are plotted in Fig. 10. Only relatively bright galaxies ($R < 21.5$) were investigated, since colours were available for all of these galaxies in the area studied. The colours were measured on images with the dominant elliptical galaxy G1 subtracted, and using fixed apertures of 4.7 arcsec diameter. The B-R colours are accurate relative to each other, but are not accurate in an absolute sense because of the lack of B band calibration.

Of the five galaxies within 200 h_{50}^{-1} kpc of the centre of the dominant elliptical galaxy (shown as filled squares in Fig. 10), three are outliers from the general distribution. Galaxy G10 (identified in Fig. 1) is the bluest of all the galaxies and has a low mean R band surface brightness. Its unusual appearance can be best seen in Fig. 5. Ignoring galaxy G4, which appears to be projected behind a foreground star, galaxy G3 has one of the highest surface brightnesses. Both of these galaxies are very close (in projection) to the central galaxy; both are within its isophotes. In addition, galaxy G11 is very red.

Although we have no redshift for galaxy G10, its location only 9 arcsec (or 35 kpc) from the centre of the dominant galaxy, and its exceptional colour and appearance argue strongly for an association between the two galaxies. Its blue colour relative to other galaxies in the field suggests recent star formation. This is not, however, a major merger. Galaxy G10 emits $< 1\%$ of the R band light of the dominant galaxy. One interpretation of the high surface brightness and small size of the other unusual nearby galaxy, G3, is that it is the high-density nuclear remains of a brighter galaxy. In

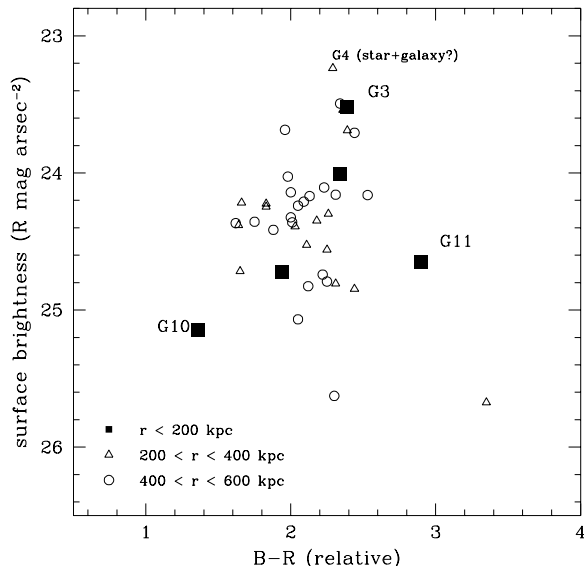


Figure 10. The properties of galaxies close to the central galaxy. Mean surface brightness is plotted against relative B-R colour for galaxies with $R < 21.5$ at a range of projected distances from the central galaxy. Three of the five galaxies within 200 kpc have fairly extreme properties, suggesting galaxy interactions are occurring.

any case, the high fraction of abnormal galaxies close to the central galaxy suggests that interactions are occurring.

3.7 Central cooling flow

The ROSAT HRI data allow an investigation of the properties of the hot X-ray emitting gas at the centre of the group, coincident with the dominant galaxy. We have performed a joint fit of all the X-ray data (PSPC spectral images and HRI image) to a model of the X-ray emitting gas, assuming hydrostatic equilibrium and a King profile for the gas density variation with radius but with the metallicity fixed at the integrated value determined by P94. The spatial and spectral instrument response functions were included as de-

scribed in Ponman & Bertram (1993). The assumption of spherical symmetry is reasonable in the core of the group. We find that the cooling time of the X-ray gas decreases with decreasing radius, and is below 10 Gyr for $r \lesssim 0.8$ arcmin ($190 h_{50}^{-1}$ kpc). The cooling time is ~ 1 Gyr for $r < 6$ arcsec. Using the method of White, Jones & Forman (1997) we derive a mass deposition rate within $r = 0.8$ arcmin of $45 M_{\odot} \text{ yr}^{-1}$ for a steady state cooling flow. However, we find no evidence of a strong decrease in the X-ray temperature at the group centre, as measured by the PSPC. This could be due to the cooling flow being young, with insufficient time for widespread cooling to set in after disruption by galaxy merging perhaps 3-4 Gyr ago. However, the rather poor PSPC spatial resolution (≈ 25 arcsec) may be blurring the observed temperature profile such that, within the limited statistical accuracy, the central temperature decrement is not observed.

4 DISCUSSION

4.1 Comparison with other groups

RXJ1340.6+4018 was selected from an X-ray survey. Poor clusters selected optically on the basis of the D or cD-like appearance of the brightest galaxy include those of Morgan, Kayser & White (1975, hereafter MKW) and Albert, White & Morgan (1978, hereafter AWM). The X-ray luminosity, X-ray temperature, velocity dispersion, mass estimates and mass/light ratio of RXJ1340.6+4018 all lie within the range of the same parameters of the MKW/AWM poor clusters (Kriss, Cioffi and Canizares 1983; Beers et al 1995; Bahcall 1980). The distribution of the galaxy optical luminosities is, however, very different in RXJ1340.6+4018.

The extreme nature of the value of $\Delta m_{12} = 2.5$ mag for RXJ1340.6+4018 can be appreciated from the comparison with the distribution of Δm_{12} in poor clusters shown in Fig. 11. The comparison samples are the 25 optically selected poor clusters of Price et al (1991) and the 15 MKW/AWM clusters of Beers et al (1995) with ≥ 6 galaxy redshifts. The mean of these distributions is $\Delta m_{12} = 0.4-0.5$. Using a different sample of 16 MKW/AWM clusters, and based on photometry alone, Bode et al (1994) quote a median Δm_{12} of 0.8 and a range of 0.1 to 1.8. The MKW/AWM clusters were selected to contain a dominant giant elliptical galaxy, and thus should have larger values of Δm_{12} than randomly selected groups, but even compared to this sample, RXJ1340.6+4018 has an extreme Δm_{12} value.

To quantify the random probability of obtaining a value of $\Delta m_{12} \geq 2.5$, we performed 14000 Monte Carlo realisations of luminosity functions with the absolute magnitudes selected at random from a Schechter function distribution. We used two of the LFs shown in Fig. 11 with extreme values of the faint end slope, and a faint limit of $M_R = -16$, as in our observations. Using the MKW/AWM composite poor cluster LF of Yamagata & Maehara (1986), which has a flat faint end slope ($\alpha = -1.07$) we found that less than 0.1% of the simulated LFs had $\Delta m_{12} \geq 2.5$. The mean and median Δm_{12} values were 0.48 and 0.38, and the Δm_{12} distribution is shown in Fig. 11. For the composite poor group LF of Ferguson & Sandage (1991), with the steepest faint end slope ($\alpha = -1.39$), a larger fraction of galaxies had faint luminosi-

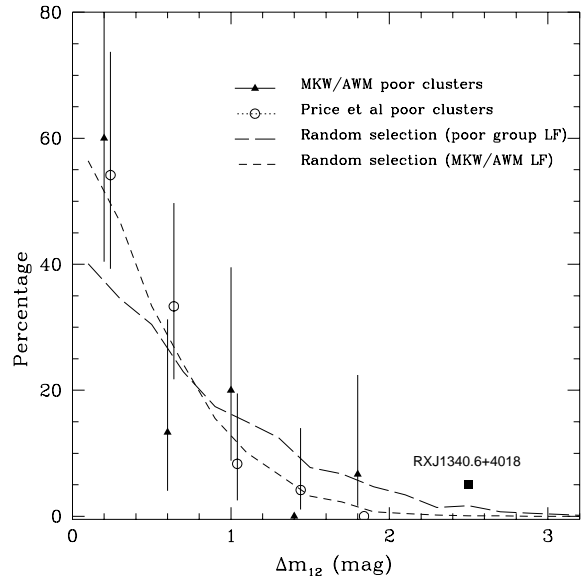


Figure 11. The distribution of Δm_{12} , the magnitude difference between the brightest and second brightest cluster galaxies. The extreme value for RXJ1340.6+4018 can be compared with values calculated from the data of Beers et al (1995) for 15 MKW/AWM poor clusters, and for the compilation of poor clusters of Price et al (1991). The ordinate is the percentage per bin of size 0.4 mag. Also shown are predictions based on random selection from two of the Schechter function LFs shown in Fig. 7.

ties, resulting in higher values of Δm_{12} (1.2% of the simulated LFs had $\Delta m_{12} \geq 2.5$). The mean and median Δm_{12} values were 0.71 and 0.55, less consistent with the observed distributions in Fig. 11.

To compare the simulated random probabilities with the number of observed systems we use the results of Jones et al (1999) who find $\approx 5\%$ of 100 X-ray selected groups and clusters in the WARPS survey have $\Delta m_{12} \geq 2.5$, together with the results of Vikhlinin et al (1999), who estimate from 4 similar systems that they comprise $\approx 20\%$ of all clusters and groups of comparable X-ray luminosity. These estimates are significantly larger than the 0.1%-1% predicted from random selection, suggesting that some other formation process is at work.

If this other process is galaxy merging, how many L^* galaxies are required to form the dominant galaxy? Given the mean M_R^* of -23.0 for the LFs in Fig. 11, the answer is ≈ 3 . Three galaxies is also consistent with the number missing from the gap in the observed LF between the first and second brightest galaxies.

A few of Hickson's compact groups (HCGs) have apparently large Δm_{12} values (eg. Fig. 11 of Prandoni et al 1994) but these are generally due to the projection of unrelated foreground galaxies on to the groups; indeed HCGs were deliberately chosen to contain at least four galaxies of similar magnitude (within 3 mag of the brightest galaxy), so the selection criteria should bias them toward low values of Δm_{12} .

Related measurements are the fraction of the total group light in the dominant galaxy and the central galaxy surface density N_0 . From the LF of Fig. 7 at $r < 400 h_{50}$ kpc

we find that $\approx 70\%$ of the group light arises from the central galaxy. We have used a limiting absolute magnitude of $M_R = -16$ to calculate this fraction but the result is valid for any absolute magnitude limit fainter than $M_R \approx -19$ because the luminosity function integral converges. By comparison, the fraction of the Virgo cluster light arising in M87 is only $\approx 5\%$, as derived from the data of Sandage, Binggeli & Tammann (1985) and using a corresponding absolute magnitude limit. The Virgo cluster bolometric X-ray luminosity is similar to that of RXJ1340.6+4018 (White, Jones & Forman 1997). The fractions of the cluster light emitted by the brightest cluster galaxies in the MKW/AWM poor clusters have intermediate values between 11% and 40% (from the data of Thuan & Romanishin 1981), and a similar range of values is found in the rich cluster data of Oemler (1976), including clusters containing cD galaxies. Thus the fraction of light in the dominant galaxy in RXJ1340.6+4018 has an extreme value compared to a wide range of other systems.

The value of the central galaxy surface density, $N_{0.5}^c$, as defined by Bahcall (1981), was measured as 2.8, assuming a richness correction appropriate for a richness class -3 group. The value for the Virgo cluster is 10 (Bahcall 1981). Abell richness class 0-1 clusters typically have $N_{0.5}^c = 10-50$.

We now make a comparison of RXJ1340.6+4018 with Hickson compact groups. RXJ1340.6+4018 is more luminous in X-rays than any of the 85 Hickson compact groups studied by Ponman et al (1996), and is a factor ~ 15 more luminous than the typical HCG detected. The group optical luminosity of RXJ1340.6+4018 is comparable to that of the brightest Hickson groups, so the L_X/L_B ratio of 0.04 is higher than any of the HCGs. In contrast, the X-ray temperature lies within the range found for HCGs by Ponman et al (1996) and RXJ1340.6+4018 lies on the $\sigma - T$ relation for HCGs.

The X-ray luminosity of RXJ1340.6+4018 is high for its X-ray temperature, and it does not lie on the $L_X - T$ relation of clusters or of groups. Fig. 12 shows the $L_X - T$ relation for clusters at $z < 0.2$ using data compiled from several sources. The solid line is the best fit using only clusters with $T > 1$ keV ($L_X \propto T^{3.13}$; Fairley et al 1999). Groups of galaxies with temperatures < 1 keV show a systematic trend to have *low* X-ray luminosities for a given temperature, as already noted by Ponman et al (1996), but RXJ1340.6+4018 has the opposite property. In fact RXJ1340.6+4018 has the largest deviation above the best fit $L_X - T$ relation of any of the clusters or groups in the plot.

4.2 The luminous central galaxy

The luminous central galaxy of RXJ1340.6+4018 does not have the characteristic envelope of cD galaxies, which would be visible as an excess surface brightness above the $r^{1/4}$ law at $\mu \lesssim 25$ mag arcsec $^{-2}$ (eg. Schombert 1986). Thuan & Romanishin (1981) found that the brightest galaxies in MKW and AWM poor clusters were also missing cD extended envelopes. They suggested that the origin of cD envelopes in rich clusters is tidally stripped matter falling on to the central galaxy, but as tidal stripping (by the cluster potential) is less efficient in groups, cD envelopes do not form there.

The total luminosity of galaxy G1 ($M_V = -23.4$) is similar to that of the brightest galaxies in the poor AWM & MKW groups studied by Thuan & Romanishin (1981) and to their estimates of the total luminosities of cD galaxies

in rich clusters, when the cD envelope luminosities were excluded.

The lack of features in the residual images after subtraction of the elliptical model in both the B and R bands shows that there are no major dust lanes in the galaxy. Thus either any dust is smoothly distributed, the progenitor galaxies were dust-free, or any dust has been sputtered by the hot X-ray gas.

With the current X-ray data we cannot separate the X-ray luminosity of the central galaxy from the X-ray luminosity of the group. Thus we cannot investigate the L_X/L_B ratio of the galaxy alone. The $\log(L_X/L_B)$ value for the group (-1.4) is $\sim 10-100$ times larger than that for normal elliptical galaxies.

4.3 Environment of the group

Because of the old ages and lack of evolution found for luminous brightest cluster galaxies (BCGs), it has been suggested that they may have formed before clusters, within groups, which then merged. It is interesting to note that RXJ1340.6+4018 lies in the outskirts of the richness class 2 cluster A1774. A1774 has a redshift of $z = 0.1691$ (Struble & Rood 1987), corresponding to a line-of-sight velocity difference of only 475 km s $^{-1}$ with RXJ1340.6+4018. The projected separation is 18.2 arcmin, corresponding to 4.1 Mpc, so RXJ1340.6+4018 is in the outskirts of A1774 and is part of the large-scale structure associated with A1774. There is no cD galaxy in A1774; the cluster has a Bautz-Morgan class of III, the class with least dominant cluster galaxies. The centre of A1774 is south of RXJ1340.6+4018 in a direction some $\approx 25^\circ$ from the X-ray position angle of galaxy G1. If RXJ1340.6+4018 is falling into A1774, then the approximate alignment of the X-ray isophotes, and probably also the dark matter distribution, with the direction of A1774, is suggestive of infall along a filamentary structure, as observed in galaxy redshift surveys and predicted in hydrodynamic simulations of large-scale structure formation (eg. Katz, Hernquist & Weinberg 1992). In a detailed N-body simulation of a poor cluster within a hierarchical cosmological model Dubinski (1998) found that after 3 Gyr (ie. by $z \approx 0.8$) the four most massive galaxies had merged along a primordial dark matter filament. The final luminous giant elliptical galaxy at the cluster core had its major axis aligned along the filament, and the appearance of the galaxies at $z=0$ was very similar to the observations presented here.

4.4 Merger age

If the central galaxy has formed via multiple mergers, then the last major merger probably occurred several Gyr ago, because there are now no morphological signs left of merging activity (boxy isophotes, shells or tidal tails). The galaxy lies on the fundamental plane, colour-magnitude and metallicity- velocity dispersion relations of normal ellipticals. The time since the last major starburst, according to the correlation of deviation from the fundamental plane with spectroscopic age of Forbes et al (1998), is $\gtrsim 4$ Gyr. An estimate of the age of the stellar population can be made using the Lick line index system as defined by Worthey (1994). Although we can not do a full correction to the Lick system,

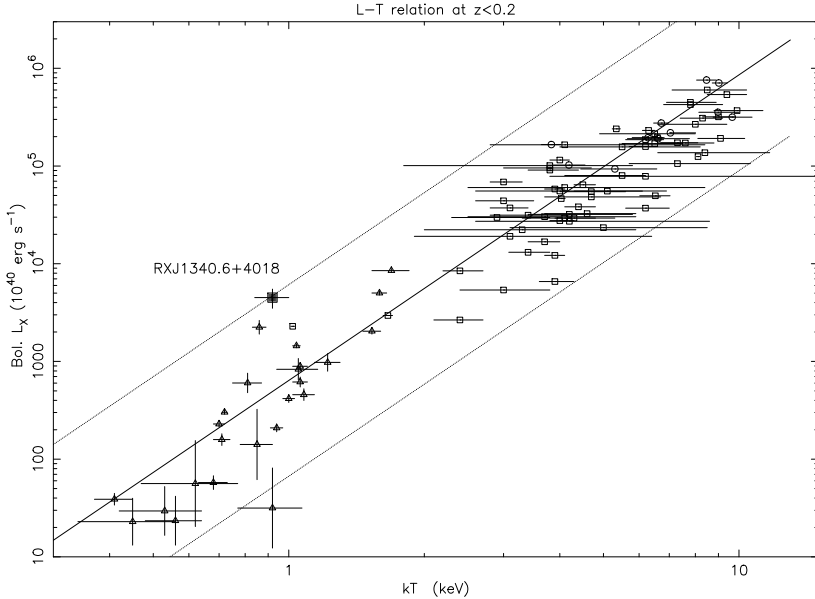


Figure 12. X-ray luminosity-temperature relation for clusters and groups. RXJ1340.6+4018 is the most deviant point above the best fit (solid) line. Dotted lines are parallel to the best fit line and are merely to guide the eye. Open squares are from David et al (1993), circles from Mushotzky & Scharf (1997) and triangles from Helsdon & Ponman (1999).

the $H\beta$ line index is sufficiently small (equivalent width= 0.8 ± 0.2 Å) to rule out a young age and is consistent with the oldest ages in the Worthey models ie. 18 Gyr.

Dynamical friction causes massive galaxies to lose energy and spiral in toward the group centre (eg. White 1976). The timescale for dynamical friction can be estimated using the equations given by Binney & Tremaine (1987) which integrate the Chandrasekhar (1943) dynamical friction force as a galaxy falls toward the group centre. Assuming the total gravitating mass is proportional to r^{-2} , consistent with our analysis of the X-ray data, and the galaxy is initially on a circular orbit of radius 200 kpc with velocity $\sqrt{2}\sigma_r$, an L^* galaxy with a typical mass/light ratio of $10 M_\odot/L_\odot$ is predicted to fall into the group centre in $\sim 4.5 \times 10^9$ yr. Thus the lack of observed L^* galaxies within a radius of 200 kpc is consistent with the effects of dynamical friction acting over a substantial fraction of a Hubble time.

4.5 Comparison with simulations

The X-ray observations of RXJ1340.6+4018 require a massive dark halo to gravitationally bind the hot X-ray gas. The fraction of dark matter initially distributed in halos around individual galaxies, rather than distributed throughout the group, is not known. Dark galaxy halos may be stripped by galaxy interactions.

In the simulations of virialized poor clusters of Bode et al (1994), if 50% of the dark matter is initially in galaxy halos, galaxy merging occurs and a dominant central galaxy is produced after $\sim 1 \times 10^{10}$ yr. Most mergers involved the dominant galaxy. This galaxy contains a third or more of the luminous matter in the cluster and accretes $0.5\text{--}5L^*$. The mass function, which was initially continuous, develops a gap of a factor ≈ 6 in mass between the most massive galaxy and the second most massive.

The similarities between the properties predicted by the simulations of Bode et al (1994) and the observed properties of RXJ1340.6+4018 are striking: the gap in the predicted mass function and the gap in our observed luminosity function (of $\Delta m_{12}=2.5$ mag or a factor of 10), the total luminosity ($\approx 3L^*$) and the high fraction of the total cluster light in the dominant galaxy.

In the same simulations, if all the dark matter is initially distributed throughout the group, the initial galaxy masses are smaller, and the dynamical friction timescales are longer. Merging is delayed beyond 13 Gyr, and a central dominant galaxy is not produced. Thus, according to these simulations (in which the dark halos were $\sim 2-4$ times more massive than the luminous matter), if merging is a dominant process, the extreme properties of the RXJ1340.6+4018 system could only be produced if galaxies initially had massive dark halos. Governato, Tozzi & Cavaliere (1996) note that the merger rate for galaxies with very massive dark matter halos (>4 times the luminous matter mass) may not be faster than for galaxies with less massive halos. In the collapse phase, included in their simulations, unequal dark matter halos are tidally stripped to about the same size and mass.

The simulations of galaxy groups of Governato, Tozzi & Cavaliere (1996) also produced a ‘merging runaway’ (Cavaliere, Colafrancesco & Menci 1991) in which a large fraction of the galaxies merged to produce one or two central massive galaxies in a few crossing times after the initial collapse of the central region. These simulations started in a non-virialized state and included galaxy infall. Governato et al. (1996) also use the Press-Schechter (1974) formalism to predict a larger fraction of systems like RXJ1340.6+4018 in an open, $\Omega=0.2$ Universe than in an $\Omega=1$ Universe. In an open Universe only 10%–15% of groups were predicted to have formed since $z=0.3$, compared to 30%–50% of groups in a critical density Universe. In the open Universe predictions

there was also little galaxy infall into groups, and group ages corresponded to a significantly larger number of crossing times than in a critical density Universe. For either value of Ω , Governato et al. (1996) found that most galaxy merging occurred at high redshifts $z > 0.3$ (and still higher redshifts for an open Universe), so the observed lack of morphological signs of merging is not surprising. The detailed properties and statistics of systems like RXJ1340.6+4018 may therefore help to constrain cosmological parameters and/or galaxy formation models.

4.6 Formation mechanisms

The large gap in the galaxy luminosity function and the very high fraction of the group light emitted by the central galaxy suggest that galaxy merging has occurred, as predicted by simulations of groups. At least one neighbouring galaxy (G10) has an extreme colour and may be interacting with the central galaxy.

However, the undisturbed, relaxed morphology of the central galaxy, its location on the fundamental plane of ellipticals and the lack of strong Balmer absorption lines in the optical spectrum show that a major merger (causing major star formation activity) has not occurred recently (within 4 Gyr). This suggests that the majority of the merging occurred at an early epoch, consistent with dynamical friction predictions which would leave only low mass galaxies merging at later times. There are other pieces of evidence that suggest the RXJ1340.6+4018 system was formed at an early epoch. The deviation of the system from the $L_X - T$ relation towards high X-ray luminosities can be explained in simple terms by an early formation epoch. At early times, the higher density of the Universe leads to a higher gas density and thus a higher X-ray luminosity (since $L_X \propto n^2$).

There are puzzles remaining though. The lack of evidence for a strong cooling flow is a puzzle if the system is old, although the spatial resolution of our X-ray data may be insufficient to resolve the central temperature decrement. The elongation of the X-ray isophotes suggests that the dark matter distribution is also elongated, and thus may not be relaxed, as would be expected in an old system. The intriguing possibility that RXJ1340.6+4018 is in a filamentary structure related to the infall of mass on to A1774 remains.

The similarity of the optical galaxy ellipticity at large radii to the X-ray ellipticity, together with the approximate alignment of the optical isophotes with the X-ray isophotes, supports the observed X-ray elongation and suggests that the stars in the outer regions of the galaxy may be responding to the *group-sized* dark matter distribution. While ellipticity increasing with radius and alignment with cluster structure may be a common feature of cD galaxies (eg. Dressler 1978), it is rarely observed in regular giant ellipticals without cD envelopes.

5 CONCLUSIONS

We have measured four concordant galaxy redshifts showing that the system RXJ1340.6+4018 is a group of galaxies. ROSAT HRI X-ray observations confirm that the X-ray emission is diffuse. The X-ray properties of the group are not unlike those of the optically selected MKW and

AWM poor clusters and groups, which were selected to have dominant giant ellipticals. However, the giant elliptical in RXJ1340.6+4018 dominates the group to an extreme degree; the second brightest galaxy is a factor of 10 less luminous ($\Delta m_{12} = 2.5$ mag), and 70% of the group optical light originates in the dominant elliptical. This large magnitude gap, combined with the poorness of the system, would make it difficult to detect in two-dimensional optical surveys. The gap in the group galaxy luminosity function occurs $\sim L^*$ and the missing luminosity is consistent with the luminosity of the dominant galaxy.

We interpret the properties of the group in terms of merging of L^* galaxies at an early epoch, leaving behind low mass galaxies, as predicted by dynamical friction. Fossil groups like RXJ1340.6+4018 may be the long sought-after descendants of HCGs.

In this interpretation, the epoch of merging must have been early ($\gtrsim 4$ Gyr ago). The undisturbed morphology of the dominant galaxy, its location on the fundamental plane of ellipticals and the lack of young star features in its optical spectrum all suggest no recent merging or star formation activity. However, the marked elongation of the X-ray isophotes is more consistent with a young, unrelaxed system. Future X-ray observations will determine the detailed structure of the system as well as any relation to the nearby cluster A1774.

Clearly more examples of groups similar to RXJ1340.6+4018 need to be found before any firm statements about their space density can be made. We are searching for similar systems in the WARPS X-ray selected survey (Scharf et al 1997, Jones et al 1998). Initial results indicate that there are indeed several similar systems. Detailed observations of these fossil systems will determine the importance of merging in galaxy groups for the formation of luminous elliptical galaxies.

6 ACKNOWLEDGEMENTS

Thanks are due to Harald Ebeling for the reduction of the Keck spectrum, Bruce Fairley for the $L_X - T$ plot and Craig Collins for help with the reduction of the HRI data. We acknowledge discussions with Robert Mann and use of the ING service observing programme on La Palma. Analysis was performed on the Birmingham node of the UK Starlink network. LRJ acknowledges support of the UK PPARC.

7 REFERENCES

- Albert C.E., White R.A., Morgan W.W., 1978, ApJ, 211, 309 (AWM).
- Bahcall N.A., 1980, ApJ, 238, L117.
- Bahcall N.A., 1981, ApJ, 247, 787.
- Barnes J., 1985, MNRAS 215, 517.
- Barnes J.E. 1989, Nature 338, 123.
- Beers T.C., Flynn K., Gebhardt K., 1990, AJ, 100, 32.
- Beers T.C., Kriessler J.R., Bird C.A., Huchra J.P. 1995, AJ, 109, 874.
- Bender R., Burstein D., Faber S.M., 1993, ApJ, 411, 153.
- Binney J., Tremaine S., 1987, Galactic Dynamics. Princeton Univ. Press, Princeton, NJ

Bessell M.S. 1979, PASP, 91, 543.

Bode P.W., Berrington R.C., Cohn H.N., Lugger P.M., 1994, ApJ, 433, 479.

Burstein D., Heiles C., 1984, ApJS, 54, 33.

Cavaliere A., Colafrancesco S., Menci N. 1991 ApJ 376, L37.

Chandrasekhar S., 1943, ApJ, 97, 255.

Christian C.A., Adams M., Barnes J.V., Butcher H., Hayes D.S., Mould J.R., Siegel M., 1985, PASP, 97, 363.

Danese L., De Zotti G., di Tullio G., 1980, A & A 82, 322.

David L.P., Slyz A., Jones C., Forman, W., Vrtilek S.D., Arnouad K.A. 1993, ApJ 412, 479.

Djorgovski S. 1985, PASP, 97, 1119.

Djorgovski S., Davis M., 1987, ApJ, 313, 59.

Draper P., Eaton N., 1996, "Starlink User Note 109: PISA"

Dressler A., 1978, ApJ 226, 55.

Dressler A., 1984, ApJ 281, 512.

Dubinski J., 1998, ApJ, 502, 141.

Faber S.M., Burstein D., Dressler A., 1977, AJ, 82, 941.

Fairley B.W., Jones L.R., Scharf, C.A., Ebeling, H., Perlman, E., Horner, D., Wegner, G., Malkan, M. 1999, in preparation.

Ferguson H.C., Sandage A., 1991, AJ, 101, 765.

Forbes D.A., Ponman T.J., Brown R.J.N., 1998, ApJ, 508, L43.

Goudfrooij P., Hansen L., Jorgensen H.E., Norgaard-Nielsen H.U., de Jong T., van den Hoek L.B., 1994, A&AS 104, 179.

Governato F., Tozzi, P., Cavaliere A., 1996, ApJ, 458, 18.

Hibbard J.E., Guhathakurta P., Van Gorkom J.H., Schweizer F., 1994, AJ, 107, 67.

Helsdon S., Ponman, T.J., 1999, MNRAS submitted.

Hunsberger S.D., Charlton J.C., Zaritsky D., 1998, ApJ, 505, 536.

Jedrzejewski R.I., 1987, MNRAS, 226, 747.

Jenkins E.B., Savage B.D., 1974, ApJ, 187, 243.

Jones L.R., Fong R., Shanks T., Ellis R.S., Peterson B.A. 1991, MNRAS, 249, 481.

Jones L.R., Scharf C.A., Ebeling H., Perlman E., Wegner G., Malkan M., Horner, D., 1998, ApJ, 495, 100.

Jones L.R. et al. 1999, in preparation.

Katz N., Hernquist L., Weinberg D.H., 1992, ApJ, 399, L109.

Kriss G.A., Cioffi D.F., Canizares C.R., 1983, ApJ, 272, 439.

Kron R.G. 1980 ApJS, 43, 305.

Landolt A.U., 1992. AJ, 104, 340.

Metcalfe N., Shanks T., Fong R., Jones L.R., 1991, MNRAS, 249, 498.

Metcalfe N., Shanks T., Fong R., Roche N., 1995, MNRAS, 273, 257.

Morgan W.W., Kayser S., White R.A., 1975, ApJ, 199, 545 (MKW).

Mulchaey J.S., Davis D.S., Mushotzky R.F., Bursstein D., 1996, ApJ, 456, 80.

Mulchaey J.S., Zabludoff, A.I., 1999, ApJ, 514, 133.

Mushotzky R.F., Scharf, C.A. 1997 ApJ, 482, L13.

Oemler A. 1976, ApJ 209, 693.

Pence W. 1976, ApJ, 203, 39.

Prandoni I., Iovino A., MacGillivray H.T., 1994, AJ 107, 1235.

Price R., Burns J.O., Duric N., Newberry M.V., 1991, AJ, 102, 14.

Ponman T.J., Bertram D., 1993, Nature, 363, 51.

Ponman T.J., Allan D.J., Jones L.R., Merrifield M., McHardy I.M., Lehto H.J., Luppino G.A. 1994, Nature, 369, 462 (P94).

Ponman T.J., Bourner, P.D.J., Ebeling, H., Bohringer H., 1996, MNRAS, 283, 690.

Press W.H., Schechter P., 1974, ApJ, 187, 425.

Prugniel Ph., Simien F., 1996, A&A, 309, 749.

Ramella M., Geller M.J., Huchra J.P. 1989, ApJ 344, 57.

Saglia R.P. et al. 1997, MNRAS, 292, 499.

Sandage A., Binggeli B., Tamman G.A., 1985, AJ, 90, 1759.

Scharf C.A., Jones L.R., Ebeling H., Perlman E., Malkan M., Wegner G. 1997, ApJ, 477, 79. Schombert J.M. 1986, ApJS, 60, 303.

Smail I., Hogg D.W., Yan L., Cohen J.G., 1995, ApJ, 449, L105.

Steidel C.C., Hamilton D., 1993, AJ, 105, 2017.

Struble M.F. Rood H.J. 1987, ApJS, 63, 543.

Thuan T.X., Romanishin W., 1981, ApJ 248, 439.

Vikhlinin A., McNamara B.R., Hornstrup A., Quintana H., Forman W., Jones C., Way C., 1999, ApJ submitted.

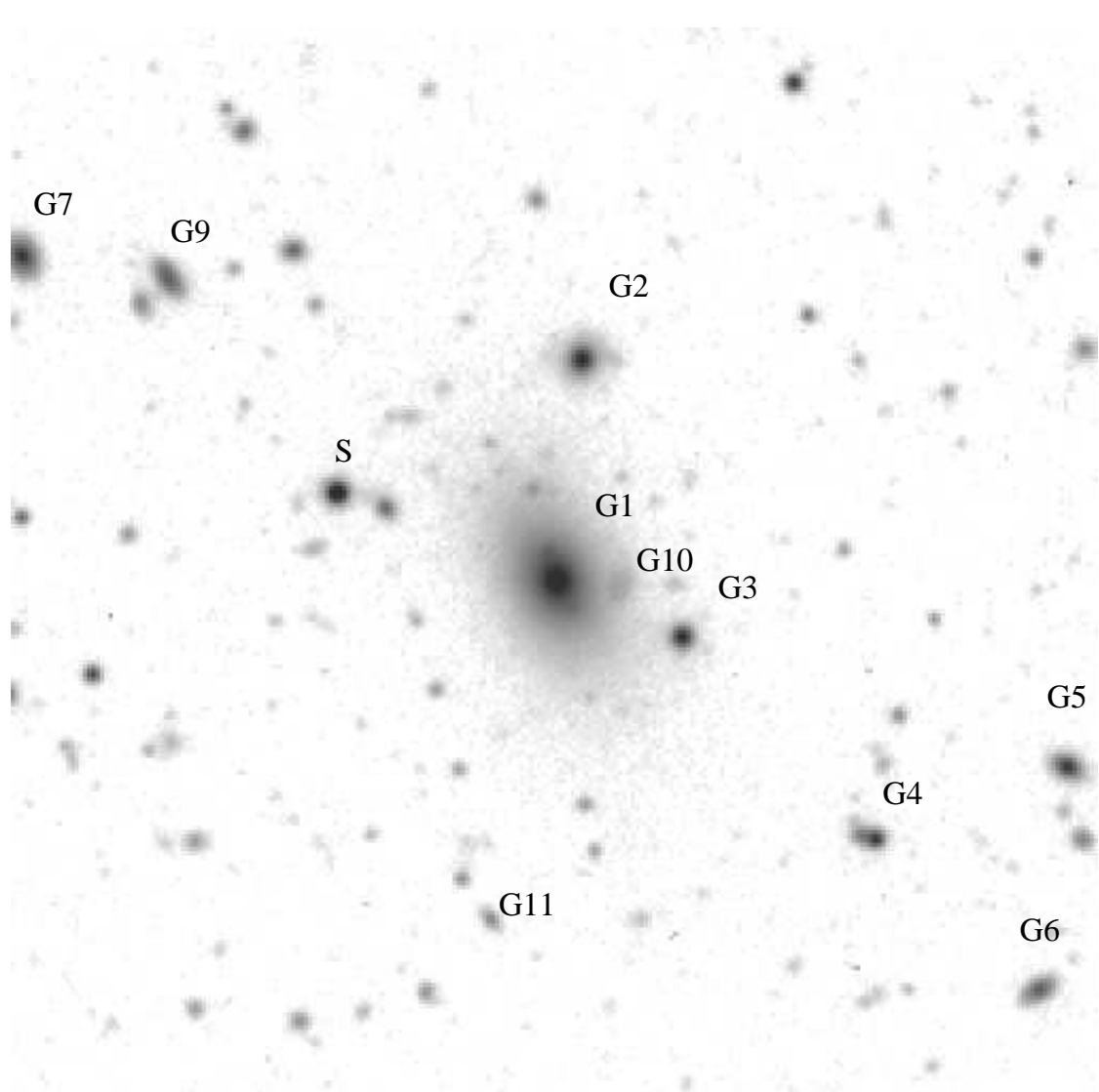
White D.A., Jones C., Forman W., 1997, MNRAS 292, 419.

White S.D.M., 1976, MNRAS, 174, 19.

Worthey G., 1994, ApJS, 95, 107.

Yamagata T., Maehara H. 1986, PASJ, 38, 661.

Zabludoff A.I., Mulchaey J.S., 1998, ApJ 496, 39.



RXJ1340.6+4018

